

Improved Liver Intravital Microscopic Imaging Using a Film-Assisted Stabilization Method

Libang Xu, Xiaobing Feng,* Dazhi Wang, Fang Gao, Chenxu Feng, Qiji Shan, Ge Wang, Fang Yang, Junfeng Zhang, Jingwei Hou, Donglei Sun,* and Tiesheng Wang*



Cite This: <https://doi.org/10.1021/acssensors.4c01464>



Read Online

ACCESS |



Metrics & More



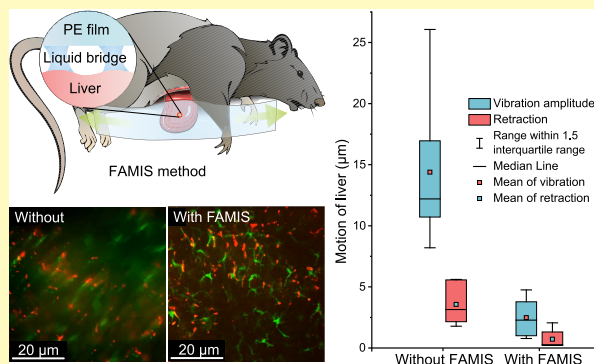
Article Recommendations



Supporting Information

ABSTRACT: Intravital microscopy (IVM) is a valuable method for biomedical characterization of dynamic processes, which has been applied to many fields such as neuroscience, oncology, and immunology. During IVM, vibration suppression is a major challenge due to the inevitable respiration and heartbeat from live animals. In this study, taking liver IVM as an example, we have unraveled the vibration inhibition effect of liquid bridges by studying the friction characteristics of a moist surface on the mouse liver. We confirmed the presence of liquid bridges on the liver through fluorescence imaging, which can provide microscale and nondestructive liquid connections between adjacent surfaces. Liquid bridges were constructed to sufficiently stabilize the liver after abdominal dissection by covering it with a polymer film, taking advantage of the high adhesion properties of liquid bridges. We further prototyped a microscope-integrated vibration-damping device with adjustable film tension to simplify the sample preparation procedure, which remarkably decreased the liver vibration. In practical application scenarios, we observed the process of liposome phagocytosis by liver Kupffer cells with significantly improved image and video quality. Collectively, our method not only provided a feasible solution to vibration suppression in the field of IVM, but also has the potential to be applied to vibration damping of precision instruments or other fields that require nondestructive "soft" vibration damping.

KEYWORDS: liver IVM, intravital microscopy, film-assisted vibration damping, liquid bridge, liposomes phagocytosis



Intravital microscopy (IVM) allows direct observation of biological processes in living animals (mostly in mice) at cellular or subcellular resolution.¹ Its capability to image individual cell dynamics^{2,3} makes it a valuable tool in neuroscience,¹ oncology,⁴ immunology,⁵ *etc.* The technique can be applied to virtually all body parts such as the lung,⁶ heart,^{7–9} kidney,¹⁰ bone,¹¹ skin,¹² and brain¹ with application scenarios covering cancer,¹³ inflammation,^{14,15} sepsis,¹⁶ host-pathogen interaction,^{17,18} and drug delivery.^{19–21}

Tissue immobilization is the key to the success of IVM. Motion artifacts (i.e., imaging artifacts) induced by vibration and tissue retraction are inevitable during IVM, leading to reduced image quality or loss of region of interest (ROI). Motion artifacts originate from breathing movement, heart beating, gastrointestinal peristalsis, *etc.* Although methods to improve image acquisition^{22,23} and processing²⁴ can be used to overcome regular or small-amplitude vibrations, direct mechanical damping methods have unparalleled advantages for the liver and intestine, as they tend to exhibit irregular and large-amplitude vibrations.²⁵ A variety of such methods have been developed for IVM, including vacuum adsorption,^{26,27} anatomical organ isolation,^{25,28,29} glue or hydrogel,^{26,30} *etc.*

Real-time intravital imaging for the liver is particularly significant for its related problems including tumor metastases,^{26,31} acute and focal injury,^{32–34} nonalcoholic fatty liver disease,¹⁵ and chronic inflammatory hepatitis.¹⁴ As an abdominal organ, the living liver acquires significant vibrations from the heart, the muscles, and the lung, which introduces apparent motion artifacts to the intravital imaging process. There are usually two types of intravital imaging for the liver: (i) abdominal dissection with the extracorporeal placement of the liver (external liver model, ELM)^{25,28,30} and (ii) window installation to the abdomen (internal liver window, ILW).^{29,35,36} Although the former can only last for a few hours, vibration can be suppressed more effectively than the ILW. Nonetheless, the ELM method suffers a significant loss in image quality due to the motion artifacts magnified under the microscope. Highly skilled personnel are also required to

Received: June 17, 2024

Revised: August 21, 2024

Accepted: August 28, 2024

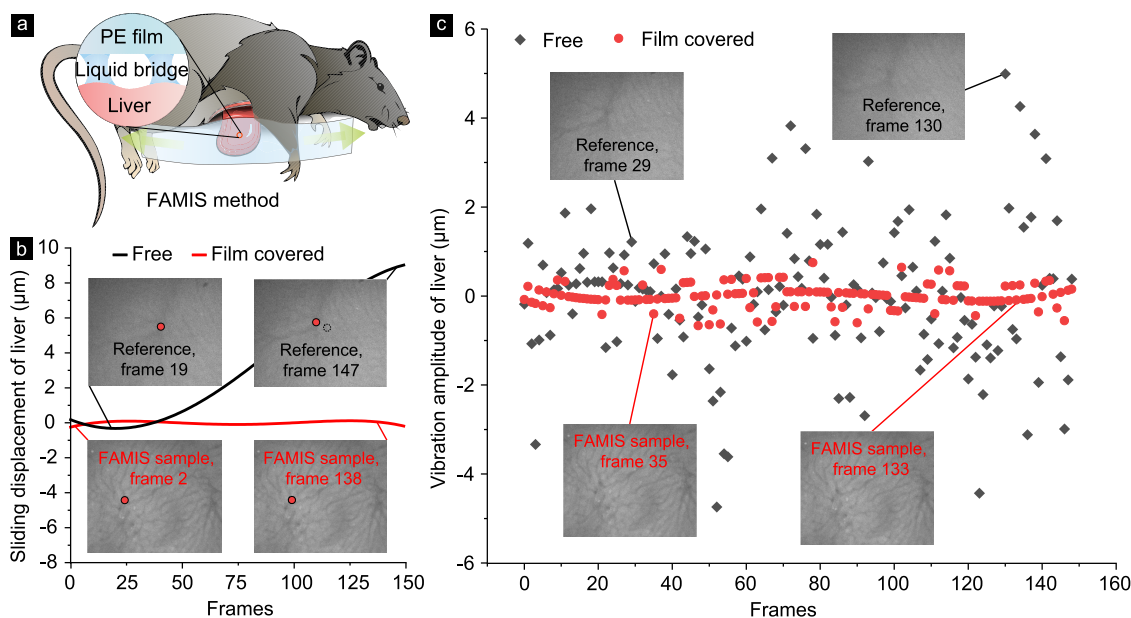


Figure 1. The FAMIS method and its impact. (a) The FAMIS method with the liver covered by a piece of PE film. (b) Retraction inhibition effect of the FAMIS method. Dashed circles are the former positions of the red dots. (c) The vibration damping effect of the FAMIS method. The two sets of data show the vibration amplitude of the liver in a restriction-free condition and covered by the PE film, respectively. Two frames of each video are taken to show the microscopic effect visible to the naked eye.

perform IVM with tolerable vibrations. There is therefore a need to develop a simple and effective method to suppress liver vibration during IVM imaging.

Here, we developed a technique to achieve sufficient vibration suppression by covering the mouse liver with a commercially available polyethylene (PE, verified in [Supporting Information Characterizations](#)) film after abdominal dissection, which was termed the film-assisted microscopic image stabilization (FAMIS) method. We have identified liquid bridges between a liver and a glass slide due to the well-known wet adhesion. These bridges are microscale liquid connections between adjacent surfaces, which can form an immobilized interface.³⁷ By covering the liver with the PE film, the liquid-bridge-immobilization mechanism was exploited to stabilize the liver during IVM ([Figure 1a](#)). We have further prototyped a microscope-integrated FAMIS device to simplify the sample preparation procedure with controllable liver-film interaction. We have demonstrated that the FAMIS method can remarkably decrease liver vibration. The level of vibration suppression can be further tuned by adjusting the tension applied to the PE film. To demonstrate the application of FAMIS, we have observed the liposome phagocytosis process in mice with significantly improved image and video quality. In the long run, the FAMIS method will not only play an important role in the field of IVM but also has the potential to be applied to vibration damping of precision instruments and suppression of organ tremor-related diseases.

EXPERIMENTAL SECTION

Materials. The following items were used as received: phosphate buffer saline (PBS, 0.01 mol/L, Share-bio), 2, 2, 2-Tribromoethanol (avertin, Acros Organics), mineral oil (Aladdin), rhodamine B (CHCIN₂O₃, 0.3 mg/mL, ADAMAS-β), and ethyl alcohol (EtOH, 75%, Sinopharm).

Animals. Six to ten-week-old C57BL/6 mice were used for all *in vivo* experiments. Mice weighing approximately 20 g were supplied by Charles Rivers. The mice were housed 5 per cage under Specific

Pathogens Free (SPF) conditions, maintaining a temperature of 23 ± 2 °C, relative humidity of $55 \pm 5\%$, and noise levels at or below 60 dB. Food and water were provided ad libitum. All protocols were approved by the Institutional Animal Care and Use Committee, IACUC at Shanghai Jiao Tong University (approval A2023221-001).

Samples Preparation of the Mouse. An adult healthy mouse, Csf1r-EGFP (MacGreen), JAX Strain #: 018549, with green fluorescent protein genes was prepared. The mouse underwent abdominal dissection, and the liver was carefully flipped out of the abdomen and immobilized in four different patterns for better access. Mouse liver L1 was free without any restriction and stayed alive during the entire IVM imaging process, while the liver samples L2 ~ L4 were fixed in different ways, including being covered with a wet tissue, covered with a film strip, and released with the film strip. Furthermore, fluorescent liposomes (FL) were administered via tail vein injection in the mouse using L1 and L3 as a basis to fabricate samples FL1 and FL2. These samples were then characterized to validate the vibration-damping efficacy of the FAMIS device under actual application conditions.

Sample Preparation of L1 ~ L4. As detailed in the abdominal dissection protocol by Kubes et al.,²⁸ we prepared forceps, scissors, a cauterizer, and other instruments ([Figure S1](#)) for the dissection of the mouse. We anesthetized the mouse and dissected the abdominal cavity, carefully exteriorizing the liver and adhering it to a glass slide to complete the preparation of sample liver L1. The specific preparation procedure is detailed in the Supporting Information FAMIS method and [Figure S2](#). The prepared sample L1 is depicted as shown in [Figure S3a](#). Samples L2 ~ L4 are prepared by restraining L1 using different methods. Among them, L2 ([Figure S3b](#)) is covered with a small piece of Kimwipes on the liver, which is what Kubes²⁸ employed. L3 ([Figure S3c](#)) is covered with a piece of a PE film strip. L4 is prepared by loosening the PE film on the liver ([Figure S3d](#)).

Samples Preparation of FL1 and FL2. The samples FL1 and FL2 were prepared by injecting the mouse sample L1 using DiI FL, where the preparation process of DiI FL is as follows. Briefly, soy bean L- α -phosphatidylcholine (PC, 20 mg), cholesterol (2 mg), and fluorophores (25 μ g DiI) were dispersed in chloroform and placed in a round-bottom flask, and then the solvent was evaporated in a rotary evaporator (at 37 °C, 100 rpm and 200 Pa). The formed thin film was hydrated at 37 °C by adding 1 X phosphate buffered saline (PBS), pH = 7.4. The suspension was dispersed by sonicating for 3 min (22 kHz)

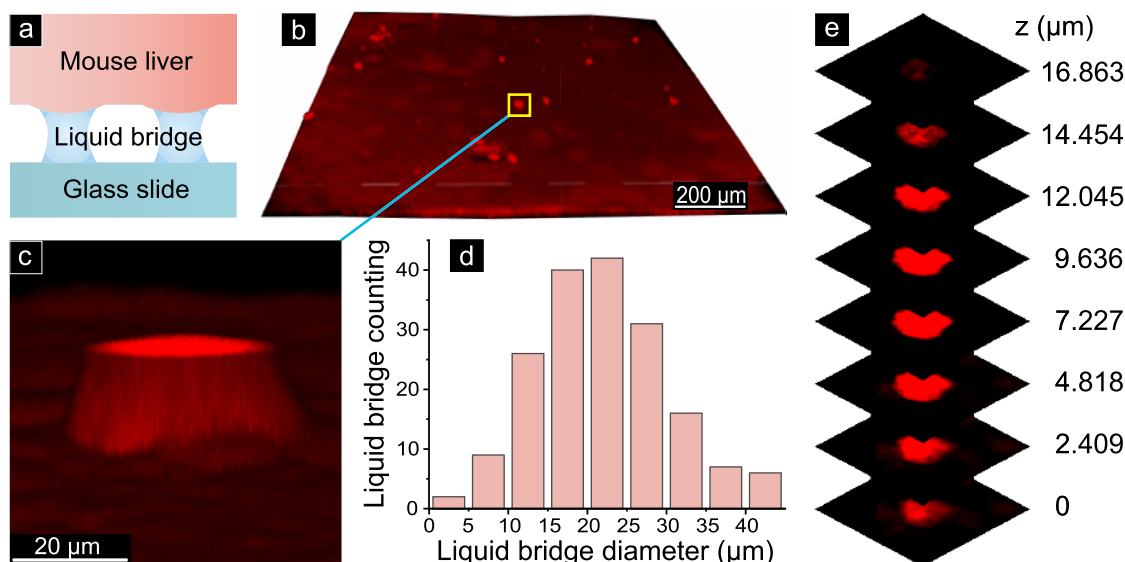


Figure 2. Liquid bridge of the liver. (a) Possible formation of liquid bridges by contact of wetted liver with glass slides in IVM. (b) Some observed liquid bridges. (c) Close-up view of the liquid bridge. (d) Observed liquid bridge diameter distribution. The rightmost bar represents 40 μm or more. (e) Layered view of the liquid bridge.

in water bath, and then homogenized by extrusion through polycarbonate membranes (Waterman) with 1.0 μm pore size. The FL samples were prepared with a total lipid concentration of 22 mg/mL in PBS (pH 7.4) for the IVM experiments.

Preparation of the FAMIS Device. The FAMIS device secures the liver by stretching the PE film covering the liver surface through a dovetail slide. For ease of operation, the roller that restrains the PE film strip is designed to flip upward and can be clamped by a buckle. Additionally, a gear rack mechanism is designed to adjust the mouse to expose as much of the liver as possible. All components and their assembly processes are displayed in Figure S4.

IVM Imaging and Observation of the Samples. Prepared samples were placed on a microscope stage for imaging. During the observation of L3, the knob was rotated to gradually stretch the PE film until the vibration amplitude of the liver was satisfactory. Thermal insulation was turned on to keep the mouse warm. Liver activities were observed, and videos were recorded. Throughout the entire sample preparation and observation process, it was necessary to moisten the liver and other organs with a cotton swab dipped in PBS every 10–15 min.

RESULTS AND DISCUSSION

Retraction Control and Vibration Damping via PE Film. Recording videos for post-event analysis is crucial for IVM imaging. We captured two sets of motion videos of the liver (Supporting Information Movie 1) from the abdominal dissected mouse: (i) liver flipped on the glass slide and restrain free (*i.e.* reference) and (ii) liver flipped on the glass slide and covered with the PE film (*i.e.* FAMIS sample). The videos consist of 149 frames each, with a duration of 15.5 s at a frame rate of 9.6 frames per second. We have observed that liver movements consist of a combination of vibration and retraction. Changes in liver position (*i.e.*, retraction) over time were tracked and fitted with exponential functions by the least-squares method, which we have termed the “retraction curve.” Any remaining liver motion that deviates from this retraction curve was categorized as a vibration. Both vibration and retraction in each video are calculated using a grayscale projection algorithm detailed in the Supporting Information FAMIS algorithm, Figure S5.

As for the retraction, the liver in the reference group retracted by 9.31 μm in 15.5 s, with a retraction rate of approximately 0.6 $\mu\text{m}/\text{s}$. Whereas the liver in the FAMIS sample group retracted only by 0.37 μm , the retraction rate of which did not exceed 0.024 $\mu\text{m}/\text{s}$ (Figure 1b). At this rate of retraction, if we consider a hypothetical field of view of $1000 \times 1000 \mu\text{m}^2$, it is estimated that over half of this field of view would be lost within 14 min in the reference group, while the typical IVM observation time is usually more than 2 h. Correspondingly, 83% of the field of view is still retained in the FAMIS sample group over 2 h. It is also evident in the figure that the liver in the reference group produces a retraction visible to the naked eye (from a dashed circle to a red dot), while the retraction of the liver in the FAMIS sample group is not obvious.

As for the vibration of the liver in the two groups (Figure 1c), the maximum amplitude of liver vibration approached 10 μm in the reference group, which can easily form motion artifacts, blurring the images. In the FAMIS sample group, the maximum vibration amplitude was controlled to approximately 1.4 μm , thereby significantly improving the clarity of the acquired IVM images.

Wet Adhesion between the Mouse Liver and the Glass. Rigid fixation with metal pieces can be damaging to the liver due to its fragile nature.^{38,39} In contrast, surface immobilization with the PE film can be less destructive. As friction is one of the effective methods of surface immobilization, we have performed a series of measurements to characterize the friction behaviors between a mouse liver and a glass microsphere (Figure S6, detailed in the Supporting Information Friction experiment). The friction experiments were conducted on a lateral force microscope (LFM, MFP-3D, detailed in Supporting Information Characterizations). One friction experiment was conducted on a moist liver surface in the air (Figure S6a), and the other was conducted with the liver immersed in water (Figure S6b). At pressures higher than 15 nN, there was a significant (about 1 order of magnitude) improvement of friction force in air over that in water (Figure

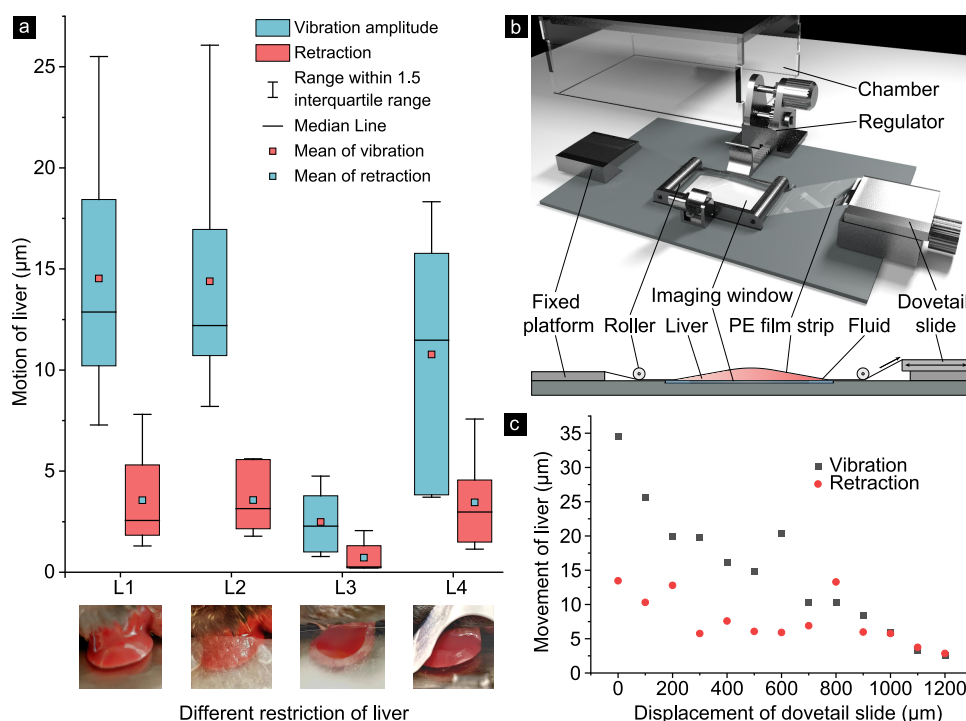


Figure 3. FAMIS device and its motion control efficacy. (a) Vibration damping and retraction control efficacy of different samples (L1–L4) (sample preparation detailed in [Supporting Information FAMIS Method](#)). (b) A prototype device with adjustable tension. (c) Amplitude recordings of the liver at different PE film tensions with a FAMIS device. The displacement of the slide is recorded to indicate the film tension.

S6c), which can be attributed to the adhesion between two wet bodies.

Wet adhesion has been broadly investigated in soft matter,⁴⁰ colloid, and interface science.^{41,42} The attraction comes from liquid bridges formed between two surfaces in proximity. The liquid bridges can exert a capillary force to form an attachment between surfaces. The behavior has been observed for bodies with either flat or curved surfaces.^{43,44} The liver surface which was removed ([Figure S6d](#)) carries body fluid, which can be used to construct liquid bridges ([Figure 2a](#)). Utilizing the capillary force of the liquid bridges, the friction in air is, therefore, much greater than that in water.

In order to verify the presence of liquid bridges, a glass coverslip was coated with a rhodamine B (excitation wavelength of 561 nm) aqueous solution. The fresh mouse liver (dissected within 0.5 h) was then placed on the glass. Rhodamine B can stain the body fluid (from the mouse liver) between the liver and the glass. A stimulated emission depletion (STED) super-resolution microscope (Leica TCS SP8 STED 3X) was used to characterize the interface between the liver and the glass ([Figure S7](#), detailed in [Supporting Information Characterizations](#)). We observed numerous liquid bridges between the liver and the glass ([Figure 2b,c](#)). Among 179 liquid bridges, the diameter ranges from 4 to 60 μm with a mean diameter of 22 μm and a median diameter of 21.82 μm ([Figure 2d](#)). Further detailed characterizations ([Figure 2e](#)) reveal a cylindrical morphology of the liquid bridge. The results match well with other liquid bridges observed in refs 45,46. Additionally, images of the liquid bridges were taken at intervals of 3 min from a fixed spot on the liver's surface, revealing a progressive fading of the liquid bridges over time ([Figure S8](#)). This fading is suspected to result from the liver's absorption of the staining agent, which corroborates the fact that the observed structures are true liquid bridges rather than

contaminants. The liquid bridges at the liver-film interface were also observed ([Figure S9](#)), providing ample theoretical support for film-based vibration damping. The component of the liver-covering film was confirmed by Fourier transform infrared spectrometry (FTIR, [Figure S10](#)) as PE ([Figure S11](#)).

Vibration Damping and Retraction Control Efficacy of the FAMIS Device. Videos of mouse liver motion under four different restraining conditions were recorded (sample preparation process and results detailed in [Supporting Information FAMIS method](#)), including freely placed on a glass slide (L1, [Figure S3a](#)), covered with a wet tissue (L2, [Figure S3b](#)), covered with a film strip (L3, [Figure S3c](#)), and with the film strip released (L4, [Figure S3d](#)). Upon analyzing the vibration amplitude across data sets L1 to L4 ([Figure 3a](#)), Group L3 demonstrates the smallest mean vibration amplitude at 2.65 μm , significantly lower than the mean values of Group L1 at 14.86 μm , Group L2 at 14.45 μm , and Group L4 at 9.15 μm . This indicates that covering the liver with the film strip is most effective in controlling vibration, with a suppression rate of approximately 85 ~ 90%. The median vibrational amplitude shows the same trend as the mean value. By calculating the standard deviations for each group, it is observed that Group L3 not only has the lowest mean and median vibration amplitudes but also exhibits the smallest standard deviation. This suggests that Group L3's statistics are tightly clustered around the mean, reflecting a high degree of stability and precision in the film-covered condition. The retraction statistics for all four groups were consistent with the vibration amplitude. The average retraction in Group L3, at 0.72 μm (0.046 $\mu\text{m/s}$), was significantly better when compared to both groups L1 and L2, and the retraction values within Group L3 remained more stable, too.

Furthermore, to investigate the influence of the tension in the film strip on liver vibration, an adjustable FAMIS device

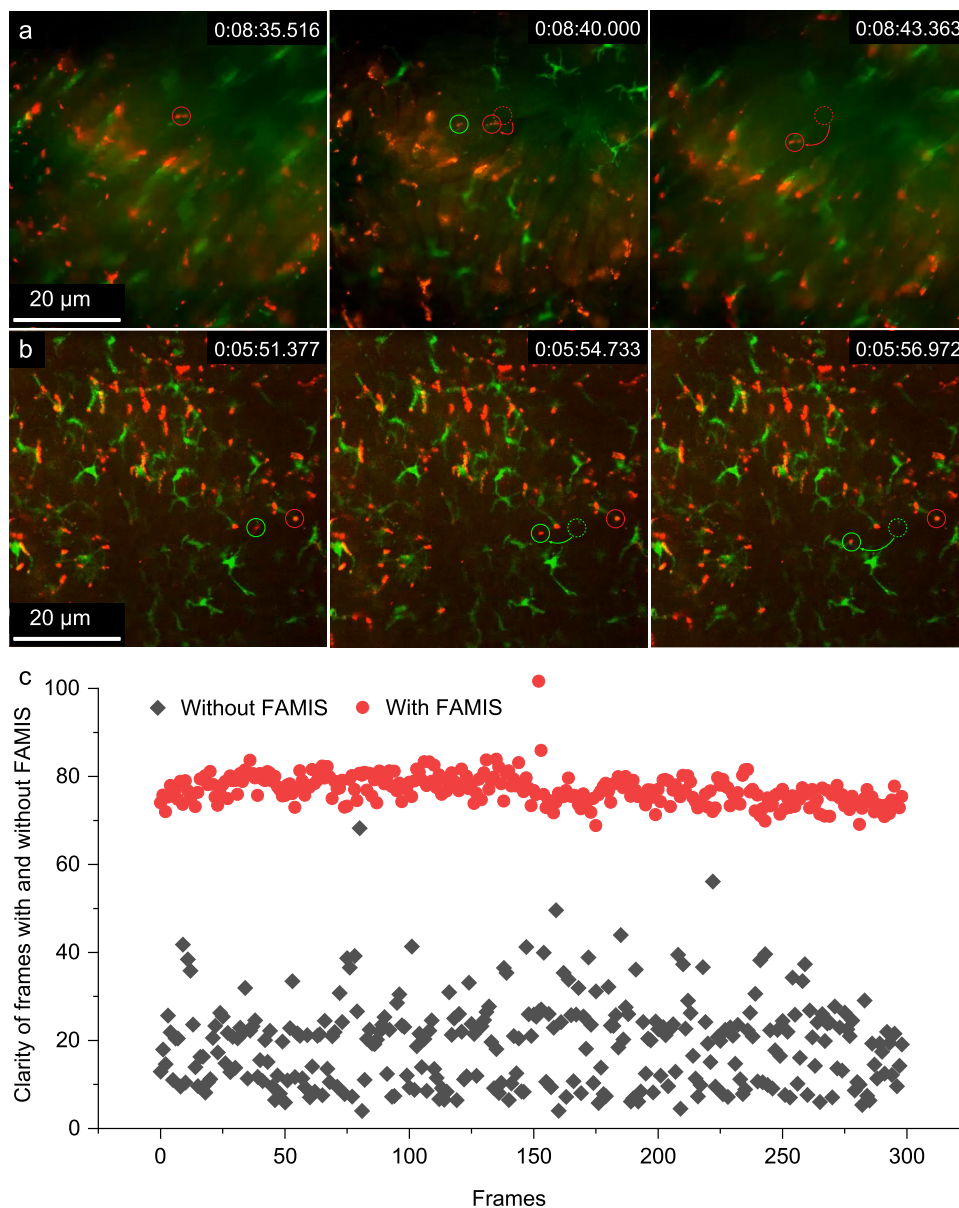


Figure 4. Characterization of FL with and without FAMIS device. (a) IVM image of FL1 without FAMIS. (b) IVM image of FL2 with FAMIS and PE film elongation of $1000\ \mu\text{m}$. The green blocks represent macrophages, and the red blocks represent liposomes. Similarly, red circles are phagocytosed and immobilized FL; green circles are uncaptured and moving FL; dashed circles are the former positions of FL. (c) Clarity of image frames with and without FAMIS device.

was designed (Figure 3b, detailed in the Supporting Information FAMIS method, Figure S4) and built with 3D-printed polylactic acid. A regulator is used to adjust the mouse's body shape and expose a larger area of the liver for easier observation. The PE film is fixed at one end, and the other end is attached to a tunable dovetail slide used to either stretch or relax the PE film strip, thereby adjusting the tightness of the PE film strip. A temperature-controlled chamber was attached to maintain the normal physiological activity of the mouse.

The vibration amplitude and retraction of the liver under various tensions were recorded while adjusting the knob of the dovetail slide (Figure 3c). A displacement of zero was recorded when the PE film was just taut. As the tension gradually increased, the motion of the liver decreased significantly. However, excessive tension could damage liver tissues and

blood vessels and reduce liver functionality. Based on our practical experience, the optimal displacement of the slide is approximately $1000\ \mu\text{m}$, considering both the liver motion control and functionality performance.

Characterization of Fluorescent Liposomes with the Support of the FAMIS Device. Liposome is one of the most commonly used drug delivery platforms because of its high biocompatibility, high biodegradability, low toxicity, and targetable nature.⁴⁷ Tracking fluorescent liposomes (FLs) under IVM is an effective way to probe nanoparticle transfer processes and elucidate drug action mechanisms.⁴⁸ Motion artifacts, however, pose a significant challenge for FL characterization. With our prototyped FAMIS device, we managed to reduce liver vibration while performing *in vivo* characterizations, confirming the unparalleled efficacy of the FAMIS method for IVM.

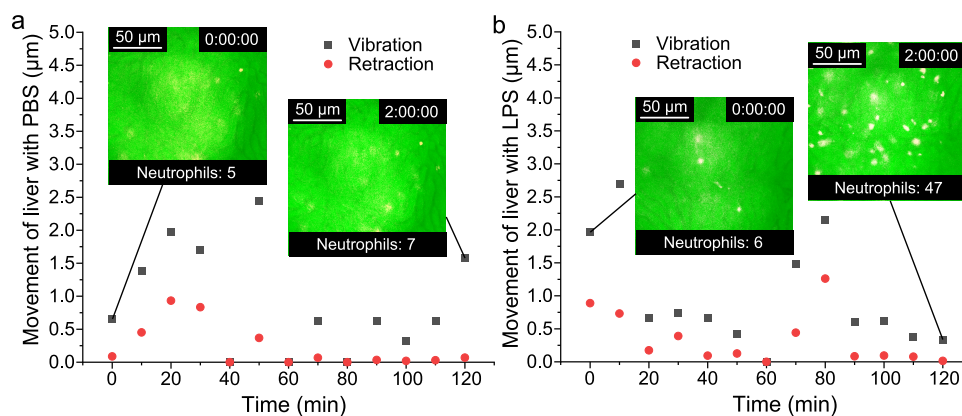


Figure 5. Long-term vibration damping of the FAMIS device and performance of its immune response. (a) Movement of mouse liver under FAMIS device with PBS and its immune responses. (b) Movement of mouse liver under FAMIS device with LPS and its immune responses. White spots represent neutrophils.

1,1'-dioctadecyl-3,3',3'-tetramethylindocarbocyanine perchlorate (DiI) FLs were used here. They were prepared by the thin-film hydration method.⁴⁹ Two experiments were conducted without the FAMIS device (FL1) and with the FAMIS device with 1000 μm PE film displacement (FL2). Both samples are prepared as detailed in the Supporting Information FAMIS method.

In FL1, the video frames produced more than 20 μm of vibration (Figure 4a, Supporting Information Movie 2). Most of the images are blurred, making it difficult to observe the phagocytosis process of FL. The phagocytosed FL exhibits intense vibrations (red circles), while the uncaptured FL fleetingly passes by (green circles). In FL2, the video has almost no visible vibration (Figure 4b, Supporting Information Movie 2). Most FL phagocytosis processes can be captured accurately in real time. The phagocytosed FL is stable, and the uncaptured FL has a recognizable motion track. Biologically, IVM imaging of FL2 confirmed that 2 h after intravenous injection FLs were mainly sequestered in Kupffer cells. More precisely, we used the Laplace operator to compute the second derivative of the image pixels as an indicator of image sharpness.^{50,51} The sharper the image, the greater the variance when it is filtered by the Laplace operator. We took 300 frames of images from each of the two sets of videos for comparison. The average sharpness of the images was 76.96 with the FAMIS device and 19.32 without (Figure 4c), indicating that effective suppression of liver motion has resulted in a significant increase in imaging sharpness and stability.

Long-Term Vibration Damping Performance of the FAMIS Device and PE Film Immunoreactivity. To verify the vibration-damping ability of the FAMIS device during a longer observation period and illustrate the immunoreactivity of the PE film, the following IVM experiments were performed with the help of the FAMIS device. Mice were injected with 2 μg of Alexa Fluor-647 conjugated anti-Ly6G mAbs (clone 1A8) via the tail vein to label neutrophils. IVM was performed to study the recruitment of neutrophils as an indicator of immunoreactivity. Ten μL of PBS was added to one liver. While ten μL of lipopolysaccharide (LPS, 10 $\mu\text{g}/\text{mL}$) solution was added topically to the other liver as a positive control. LPS is a well-known component of bacteria that can trigger neutrophil recruitment. Both livers were observed under IVM for 2 h, during which 10 s videos of the same area of the liver were recorded every ten minutes. The average liver vibration

and retraction amplitudes were effectively controlled at approximately 1 and 0.3 μm (Figure 5a,b), respectively, within two hours in both groups, presenting no significant increasing trend.

The neutrophil recruitment in the PBS group remained minimal over time (Figure 5a), while the neutrophil recruitment increased drastically in the LPS-treated group (Figure 5b), demonstrating that the PE film covering the liver induces negligible immune responses. Actually, polyethylene has been extensively applied to the fabrication of porous high-density polyethylene implants for facial and cranial reconstruction etc.,⁵² which reflects its superior biocompatibility.

Furthermore, we also found some other promising materials for the film. For example, chitosan has excellent biocompatibility and bacteriostatic properties as a wound dressing,^{53,54} which makes it suitable for IVM imaging scenarios with high aseptic requirements. Polyvinyl alcohol also has good biocompatibility, and its malleable, self-adhesive, and self-repairing properties⁵⁵ may allow it to conform more closely to the curved surface of the liver to build stronger liquid bridges to dampen organ vibration more effectively. Both materials have good film-forming and electrospinning properties.^{56,57}

Both vibration and retraction of the liver have been effectively controlled with the proposed method, resulting in improved clarity and stability for IVM. Currently, there exist several ELM-type IVM imaging methods. The agarose-based method proposed by Felix Heymann³⁰ may pose a risk of toxic substances. The methods used by Pedro E Marques²⁵ and Paul Kubes²⁸ exhibit limitations in motion reduction and difficulties in dissection. Based on the protocol of live mouse microscopy by Paul Kubes, we introduced a PE film to IVM imaging, using the liquid bridge at the film-liver interface to further suppress liver motion, controlling the vibration amplitude to around 2.65 μm (compared to 14.45 μm when the liver is unconstrained) and the retraction speed to around 0.046 $\mu\text{m}/\text{s}$ with an inhibition rate of about 90%. The method described in this paper not only introduces a "PE film" for soft constraint, which can effectively suppress liver motion, but also eliminates the time-consuming and labor-intensive process of the xiphoid tying process as described by Kubes et al., as well as the step of cutting the mesentery that can easily lead to major bleeding. In addition, we have designed and constructed an adjustable 3D-printed operating platform compatible with the microscope, easily obtainable in the laboratory, coupled

with algorithms for vibration quantification and clarity quantification (which have not yet received attention in current liver IVM imaging), making the process of live mouse liver microscopy cleaner, easier, and more professional.

Nonetheless, further work is required to improve the optimal film-covered vibration-damping solution of the mouse liver. A method to characterize liver functionality during IVM could be developed to assist in determining the optimal film tension for various observation durations, thus making FAMIS for IVM more efficient and practical. Furthermore, other factors such as film shape and size, modulus of elasticity, and surface properties may affect the vibration suppression efficacy. Other polymers and elastomers can be applied as film materials for FAMIS in the near future. Additionally, the FAMIS method can be extended to other mammals such as rats and rabbits in fields including but not limited to medicine, pharmacy, and oncology.

CONCLUSIONS

In this study, we not only discovered the phenomenon of significantly increased friction on the moist liver surface using LFM but also observed the existence of liquid bridges at the liver-glass interface and liver-PE film interface using fluorescence staining on CLSM. Considering that liquid bridges can provide strong adhesive force without damaging the liver, we innovatively proposed the FAMIS method by covering the liver with a PE film and constructing more liquid bridges to reduce liver motion, including both vibration and retraction. The quantification of these two types of motion is achieved by a grayscale projection algorithm, which has not received much attention in the IVM imaging process. As a result, the vibration amplitude was decreased to around 2.65 μm from 14.45 μm , and the retraction speed was suppressed to around 0.046 $\mu\text{m/s}$ with an inhibition rate of about 90%.

We have developed a 3D-printed FAMIS device centered around the film-covering method, aiming to sufficiently reduce liver motion and reduce the difficulty of dissection to prepare IVM imaging samples more conveniently. The FAMIS device is equipped with a regulator to adjust the posture of the mouse to expose as much of the mouse's liver as possible, and it can quantitatively adjust the tension of the PE film according to usage requirements to maximally suppress liver motion while ensuring liver functionality. The recommended tension is to adjust the dovetail slide to move outward by approximately 1 mm after the film strip is just taut. The FAMIS device has also withstood the test of practical application scenarios. In the FL characterization experiment, the mouse liver, which was dampened by the FAMIS device, showed no visible movement under the microscope at a sharpness level of 76.96, significantly higher than the 19.32 observed without the device. This enabled clear observation of the liposomes being phagocytosed by Kupffer cells.

In summary, the vibration quantification and FAMIS method discussed in this article have effectively addressed the issue of liver motion during the ELM type IVM imaging of the mouse liver. In the future, our FAMIS methods will play an important role in the field of IVM imaging for neuroscience, oncology, and immunology not only on mice but also on other small animals such as rats, rabbits, birds, and amphibians. Moreover, the method is not limited to the liver and can be extended to other organs, such as skin, intestine, and adipose tissues. Apart from biology, it also has the potential to be applied to "soft control" scenes such as vibration damping of

precision instruments or even developed into a standardized, one-stop vibration damping method similar to that of Paul Kubens.

ASSOCIATED CONTENT

Supporting Information

The Supporting Information is available free of charge at <https://pubs.acs.org/doi/10.1021/acssensors.4c01464>.

Supporting Information Movie 1 about comparison of mouse liver motion before and after covering the PE film (MP4)

Supporting Information Movie 2 about characterization of FL before and after covering the PE film (MP4)

Supporting Information_20240821 about details of FAMIS method; FAMIS algorithm; friction experiment and characterizations; SI python scripts about algorithms for vibration; retraction and image sharpness detection (PDF)

AUTHOR INFORMATION

Corresponding Authors

Tiesheng Wang – Key Laboratory for Micro/Nano Technology and System of Liaoning Province, Dalian University of Technology, Dalian 116024, China; orcid.org/0000-0001-7587-7681; Email: wangts@dlut.edu.cn

Xiaobing Feng – School of Mechanical Engineering, Shanghai Jiao Tong University, Shanghai 200240, China; Email: xiaobing.feng@sjtu.edu.cn

Donglei Sun – School of Life Sciences and Biotechnology, Shanghai Jiao Tong University, Shanghai 200240, China; Email: dongleisun@sjtu.edu.cn

Authors

Libang Xu – School of Mechanical Engineering, Shanghai Jiao Tong University, Shanghai 200240, China; orcid.org/0009-0000-3049-4230

Dazhi Wang – Key Laboratory for Micro/Nano Technology and System of Liaoning Province, Dalian University of Technology, Dalian 116024, China

Fang Gao – Department of No.1 Operating Room, Dalian Municipal Central Hospital Affiliated to Dalian University of Technology, Dalian 116024, China

Chenxu Feng – School of Life Sciences and Biotechnology, Shanghai Jiao Tong University, Shanghai 200240, China

Qiji Shan – Instrumental Analysis Center, Shanghai Jiao Tong University, Shanghai 200240, China

Ge Wang – School of Life Sciences and Biotechnology, Shanghai Jiao Tong University, Shanghai 200240, China

Fang Yang – School of Life Sciences and Biotechnology, Shanghai Jiao Tong University, Shanghai 200240, China

Junfeng Zhang – Department of Medical Equipment, Ningcheng Traditional Chinese and Mongolian Medicine Hospital, Chifeng 024200, China

Jingwei Hou – School of Chemical Engineering, University of Queensland, St Lucia, QLD 4072, Australia; orcid.org/0000-0001-9139-9835

Complete contact information is available at: <https://pubs.acs.org/10.1021/acssensors.4c01464>

Author Contributions

The manuscript is written through contributions of all authors. All authors have given approval to the final version of the manuscript. T.W., D.S., X.F., and L.X. conceived the idea about FAMIS for improved liver IVM. L.X. designed and prototyped the FAMIS system under the supervision of T.W., X.F., and D.S. L.X., C.F., G.W., and F.Y. prepared all of the samples and completed the preliminary experimental study related to FAMIS. Q.S. and L.X. carried out the friction measurements and liquid bridge characterization guided by D.W., T.W., X.F., D.S., and J.H. C.F. and L.X. obtained the results about liposome phagocytosis instructed by D.S., F.G., and Y.Z. L.X. prepared the initial manuscript instructed by T.W., D.S., X.F., and J.H. with input from all of the authors.

Notes

The authors declare no competing financial interest.

ACKNOWLEDGMENTS

The work is supported by the National Natural Science Foundation of China (Grant Number: 52103224, T.W.; Grant Number: 52105524, X.F.; Grant Number: 32100723, D.S.; Grant Number: 62074138, D.W.), the Fundamental Research Funds for the Central Universities (Grant Number: DUT23RC(3)051, T.W.; Grant Number: DUT22LAB405, D.W.), and Shanghai Municipal Commission of Science and Technology (Shanghai Sailing Program, Grant Number: No. 20YF1420400, T.W.; Shanghai Natural Science Foundation, Grant Number: 21ZR1432600, D.S.). The authors also thank Liaoning Huanghai Laboratory for funding.

REFERENCES

- (1) Streich, L.; Boffi, J. C.; Wang, L.; Alhalaseh, K.; Barbieri, M.; Rehm, R.; Deivasigamani, S.; Gross, C. T.; Agarwal, A.; Prevedel, R. High-Resolution Structural and Functional Deep Brain Imaging Using Adaptive Optics Three-Photon Microscopy. *Nat. Methods* **2021**, *18* (10), 1253–1258.
- (2) Wu, J.; Lu, Z.; Jiang, D.; Guo, Y.; Qiao, H.; Zhang, Y.; Zhu, T.; Cai, Y.; Zhang, X.; Zhanghao, K.; et al. Iterative Tomography with Digital Adaptive Optics Permits Hour-Long Intravital Observation of 3D Subcellular Dynamics at Millisecond Scale. *Cell* **2021**, *184* (12), 3318–3332.e17.
- (3) Aguirre, A. D.; Vinegoni, C.; Sebas, M.; Weissleder, R. Intravital Imaging of Cardiac Function at the Single-Cell Level. *Proc. Natl. Acad. Sci.* **2014**, *111* (31), 11257–11262.
- (4) Dai, J.; Cimino, P. J.; Gouin, K. H.; Grzelak, C. A.; Barrett, A.; Lim, A. R.; Long, A.; Weaver, S.; Saldin, L. T.; Uzamere, A.; et al. Astrocytic Laminin-211 Drives Disseminated Breast Tumor Cell Dormancy in Brain. *Nat. Cancer* **2022**, *3* (1), 25–42.
- (5) Ohta, Y.; Fujii, M.; Takahashi, S.; Takano, A.; Nanki, K.; Matano, M.; Hanyu, H.; Saito, M.; Shimokawa, M.; Nishikori, S.; et al. Cell–Matrix Interface Regulates Dormancy in Human Colon Cancer Stem Cells. *Nature* **2022**, *608* (7924), 784–794.
- (6) Neupane, A. S.; Willson, M.; Chojnacki, A. K.; Castanheira, F. V. E. S.; Morehouse, C.; Carestia, A.; Keller, A. E.; Peiseler, M.; DiGiandomenico, A.; Kelly, M. M.; et al. Patrolling Alveolar Macrophages Conceal Bacteria from the Immune System to Maintain Homeostasis. *Cell* **2020**, *183* (1), 110–125.e11.
- (7) González-Rosa, J. M.; Guzmán-Martínez, G.; Marques, I. J.; Sánchez-Iranzo, H.; Jiménez-Borreguero, L. J.; Mercader, N. Use of Echocardiography Reveals Reestablishment of Ventricular Pumping Efficiency and Partial Ventricular Wall Motion Recovery upon Ventricular Cryoinjury in the Zebrafish. *PLoS One* **2014**, *9* (12), No. e115604.
- (8) Vinegoni, C.; Aguirre, A. D.; Lee, S.; Weissleder, R. Imaging the Beating Heart in the Mouse Using Intravital Microscopy Techniques. *Nat. Protoc.* **2015**, *10* (11), 1802–1819.
- (9) Kempf, T.; Zarbock, A.; Widera, C.; Butz, S.; Stadtmann, A.; Rossaint, J.; Bolomini-Vittori, M.; Korf-Klingebiel, M.; Napp, L. C.; Hansen, B.; et al. GDF-15 Is an Inhibitor of Leukocyte Integrin Activation Required for Survival after Myocardial Infarction in Mice. *Nat. Med.* **2011**, *17* (5), 581–588.
- (10) Polesel, M.; Kaminska, M.; Haenni, D.; Bugarski, M.; Schuh, C.; Jankovic, N.; Kaech, A.; Mateos, J. M.; Berquez, M.; Hall, A. M. Spatiotemporal Organisation of Protein Processing in the Kidney. *Nat. Commun.* **2022**, *13* (1), No. 5732.
- (11) McDonald, M. M.; Khoo, W. H.; Ng, P. Y.; Xiao, Y.; Zamerli, J.; Thatcher, P.; Kyaw, W.; Pathmanandavel, K.; Grootveld, A. K.; Moran, I.; et al. Osteoclasts Recycle via Osteomorphs during RANKL-Stimulated Bone Resorption. *Cell* **2021**, *184* (5), 1330–1347.e13.
- (12) Jiang, D.; Christ, S.; Correa-Gallegos, D.; Ramesh, P.; Kalgudde Gopal, S.; Wannemacher, J.; Mayr, C. H.; Lupperger, V.; Yu, Q.; Ye, H.; et al. Injury Triggers Fascia Fibroblast Collective Cell Migration to Drive Scar Formation through N-Cadherin. *Nat. Commun.* **2020**, *11* (1), No. 5653.
- (13) Paul, C. D.; Mistriotis, P.; Konstantopoulos, K. Cancer Cell Motility: Lessons from Migration in Confined Spaces. *Nat. Rev. Cancer* **2017**, *17* (2), 131–140.
- (14) D’Mello, C.; Swain, M. G. Liver–Brain Interactions in Inflammatory Liver Diseases: Implications for Fatigue and Mood Disorders. *Brain, Behav., Immun.* **2014**, *35*, 9–20.
- (15) Malehmir, M.; Pfister, D.; Gallage, S.; Szydlowska, M.; Inverso, D.; Kotsiliti, E.; Leone, V.; Peiseler, M.; Surewaard, B. G. J.; Rath, D.; et al. Platelet GPIIb α Is a Mediator and Potential Interventional Target for NASH and Subsequent Liver Cancer. *Nat. Med.* **2019**, *25* (4), 641–655.
- (16) Schmidt, E. P.; Yang, Y.; Janssen, W. J.; Gandjeva, A.; Perez, M. J.; Barthel, L.; Zemans, R. L.; Bowman, J. C.; Koyanagi, D. E.; Yunt, Z. X.; et al. The Pulmonary Endothelial Glycocalyx Regulates Neutrophil Adhesion and Lung Injury during Experimental Sepsis. *Nat. Med.* **2012**, *18* (8), 1217–1223.
- (17) De Niz, M.; Meibalan, E.; Mejia, P.; Ma, S.; Brancucci, N. M. B.; Agop-Nersesian, C.; Mandt, R.; Ngotho, P.; Hughes, K. R.; Waters, A. P.; et al. Plasmodium Gametocytes Display Homing and Vascular Transmigration in the Host Bone Marrow. *Sci. Adv.* **2023**, *4* (5), No. eaat3775.
- (18) Rudlaff, R. M.; Kraemer, S.; Strega, V. A.; Dvorin, J. D. An Essential Contractile Ring Protein Controls Cell Division in Plasmodium Falciparum. *Nat. Commun.* **2019**, *10* (1), No. 2181.
- (19) Lin, Q.; Fathi, P.; Chen, X. Nanoparticle Delivery in Vivo: A Fresh Look from Intravital Imaging. *EBioMedicine* **2020**, *59*, No. 102958.
- (20) Jiang, Y.; Huang, J.; Zhen, X.; Zeng, Z.; Li, J.; Xie, C.; Miao, Q.; Chen, J.; Chen, P.; Pu, K. A Generic Approach towards Afterglow Luminescent Nanoparticles for Ultrasensitive in Vivo Imaging. *Nat. Commun.* **2019**, *10* (1), No. 2064.
- (21) Lam, F. C.; Morton, S. W.; Wyckoff, J.; Vu Han, T. L.; Hwang, M. K.; Maffa, A.; Balkanska-Sinclair, E.; Yaffe, M. B.; Floyd, S. R.; Hammond, P. T. Enhanced Efficacy of Combined Temozolomide and Bromodomain Inhibitor Therapy for Gliomas Using Targeted Nanoparticles. *Nat. Commun.* **2018**, *9* (1), No. 1991.
- (22) Kelly, A.; Salerno, S.; Connolly, A.; Bishop, M.; Charpentier, F.; Stølen, T.; Smith, G. L. Normal Interventricular Differences in Tissue Architecture Underlie Right Ventricular Susceptibility to Conduction Abnormalities in a Mouse Model of Brugada Syndrome. *Cardiovasc. Res.* **2018**, *114* (5), 724–736.
- (23) Lee, S.; Vinegoni, C.; Sebas, M.; Weissleder, R. Automated Motion Artifact Removal for Intravital Microscopy, without a Priori Information. *Sci. Rep.* **2014**, *4* (1), No. 4507.
- (24) Haft-Javaherian, M.; Fang, L.; Muse, V.; Schaffer, C. B.; Nishimura, N.; Sabuncu, M. R. Deep Convolutional Neural Networks for Segmenting 3D in Vivo Multiphoton Images of Vasculature in Alzheimer Disease Mouse Models. *PLoS One* **2019**, *14* (3), No. e0213539.
- (25) Marques, P. E.; Antunes, M. M.; David, B. A.; Pereira, R. V.; Teixeira, M. M.; Menezes, G. B. Imaging Liver Biology in Vivo Using

- Conventional Confocal Microscopy. *Nat. Protoc.* **2015**, *10* (2), 258–268.
- (26) Tanaka, K.; Morimoto, Y.; Toiyama, Y.; Okugawa, Y.; Inoue, Y.; Uchida, K.; Kimura, K.; Mizoguchi, A.; Kusunoki, M. Intravital Dual-Colored Visualization of Colorectal Liver Metastasis in Living Mice Using Two Photon Laser Scanning Microscopy. *Microsc. Res. Tech.* **2012**, *75* (3), 307–315.
- (27) Entenberg, D.; Rodriguez-Tirado, C.; Kato, Y.; Kitamura, T.; Pollard, J. W.; Condeelis, J. In Vivo Subcellular Resolution Optical Imaging in the Lung Reveals Early Metastatic Proliferation and Motility. *Intravital* **2015**, *4* (3), 1–11.
- (28) Babes, L.; Kubes, P. Visualizing the Tumor Microenvironment of Liver Metastasis by Spinning Disk Confocal Microscopy. In *The Tumor Microenvironment, Methods in Molecular Biology*; Humana Press: New York, 2016; Vol. 1458, pp 203–215.
- (29) Deng, D.; Dai, B.; Wei, J.; Yuan, X.; Yang, X.; Qi, S.; Zhang, Z. A Drawer-Type Abdominal Window with an Acrylic/Resin Coverslip Enables Long-Term Intravital Fluorescence/Photoacoustic Imaging of the Liver. *Nanophotonics* **2021**, *10* (12), 3369–3381.
- (30) Heymann, F.; Niemietz, P. M.; Peusquens, J.; Ergen, C.; Kohlhepp, M.; Mossanen, J. C.; Schneider, C.; Vogt, M.; Tolba, R. H.; Trautwein, C. Long Term Intravital Multiphoton Microscopy Imaging of Immune Cells in Healthy and Diseased Liver Using CXCR6.Gfp Reporter Mice. *J. Vis. Exp.* **2015**, *2015* (97), No. 52607.
- (31) Ritsma, L.; Steller, E. J. A.; Beerling, E.; Loomans, C. J. M.; Zomer, A.; Gerlach, C.; Vriskoop, N.; Seinstra, D.; van Gorp, L.; Schäfer, R.; et al. Intravital Microscopy Through an Abdominal Imaging Window Reveals a Pre-Micrometastasis Stage During Liver Metastasis. *Sci. Transl. Med.* **2012**, *4* (158), No. 158ra145.
- (32) Marques, P. E.; Oliveira, A. G.; Pereira, R. V.; David, B. A.; Gomides, L. F.; Saraiva, A. M.; Pires, D. A.; Novaes, J. T.; Patricio, D. O.; Cisalpino, D.; et al. Hepatic DNA Deposition Drives Drug-Induced Liver Injury and Inflammation in Mice. *Hepatology* **2015**, *61* (1), 348–360.
- (33) Wang, J.; Hossain, M.; Thanabalasuriar, A.; Gunzer, M.; Meininger, C.; Kubes, P. Visualizing the Function and Fate of Neutrophils in Sterile Injury and Repair. *Science* **2017**, *358* (6359), 111–116.
- (34) McDonald, B.; Pittman, K.; Menezes, G. B.; Hirota, S. A.; Slaba, I.; Waterhouse, C. C. M.; Beck, P. L.; Muruve, D. A.; Kubes, P. Intravascular Danger Signals Guide Neutrophils to Sites of Sterile Inflammation. *Science* **2010**, *330* (6002), 362–366.
- (35) Liu, Y.; Chen, H. C.; Yang, S. M.; Sun, T. L.; Lo, W.; Chiou, L. L.; Huang, G. T.; Dong, C. Y.; Lee, H. S. Visualization of Hepatobiliary Excretory Function by Intravital Multiphoton Microscopy. *J. Biomed. Opt.* **2007**, *12* (1), No. 014014.
- (36) Brown, C. M.; Rivera, D. R.; Ouzounov, D. G.; Webb, W. W.; Xu, C.; Pavlova, I. P.; Williams, W. O.; Mohanan, S. In Vivo Imaging of Unstained Tissues Using a Compact and Flexible Multiphoton Microendoscope. *J. Biomed. Opt.* **2012**, *17* (4), 1–4.
- (37) Hwang, J. K.; Cho, S.; Dang, J. M.; Kwak, E. B.; Song, K.; Moon, J.; Sung, M. M. Direct Nanoprinting by Liquid-Bridge-Mediated Nanotransfer Moulding. *Nat. Nanotechnol.* **2010**, *5* (10), 742–748.
- (38) Yin, M.; Woollard, J.; Wang, X.; Torres, V. E.; Harris, P. C.; Ward, C. J.; Glaser, K. J.; Manduca, A.; Ehman, R. L. Quantitative Assessment of Hepatic Fibrosis in an Animal Model with Magnetic Resonance Elastography. *Magn. Reson. Med.* **2007**, *58* (2), 346–353.
- (39) Ojha, S.; Pribyl, J.; Klimovic, S.; Hadraba, D.; Jirouskova, M.; Gregor, M. Measurement of Liver Stiffness Using Atomic Force Microscopy Coupled with Polarization Microscopy. *JoVE* **2022**, No. 185, No. e63974.
- (40) Chan, S. T.; Varchanis, S.; Haward, S. J.; Shen, A. Q. Torsional Instability of Constant Viscosity Elastic Liquid Bridges. *Soft Matter* **2022**, *18* (10), 1965–1977.
- (41) Haynes, M.; Vega, E. J.; Herrada, M. A.; Benilov, E. S.; Montanero, J. M. Stabilization of Axisymmetric Liquid Bridges through Vibration-Induced Pressure Fields. *J. Colloid Interface Sci.* **2018**, *513*, 409–417.
- (42) Choi, S. W.; Lee, D. E.; Lee, W. Il.; Kim, H. S. Analysis of Coalescence Behavior for Compressed Droplets. *Appl. Surf. Sci.* **2017**, *397*, 57–69.
- (43) Nguyen, H. N. G.; Millet, O.; Zhao, C. F.; Gagneux, G. Theoretical and Experimental Study of Capillary Bridges between Two Parallel Planes. *Eur. J. Environ. Civ. Eng.* **2022**, *26* (3), 1198–1208.
- (44) Chen, Y.; Zhao, Y.; Gao, H.; Zheng, J. Liquid Bridge Force between Two Unequal-Sized Spheres or a Sphere and a Plane. *Particuology* **2011**, *9* (4), 374–380.
- (45) Lehnert, M. S.; Reiter, K. E.; Bennett, A.; Gerard, P. D.; Wei, Q. H.; Byler, M.; Yan, H.; Lee, W. K. The Ingestion of Fluorescent, Magnetic Nanoparticles for Determining Fluid-Uptake Abilities in Insects. *JoVE* **2017**, No. 130, No. e56619.
- (46) Monaenkova, D.; Lehnert, M. S.; Andruk, T.; Beard, C. E.; Rubin, B.; Tokarev, A.; Lee, W. K.; Adler, P. H.; Kornev, K. G. Butterfly Proboscis: Combining a Drinking Straw with a Nanosponge Facilitated Diversification of Feeding Habits. *J. R. Soc., Interface* **2012**, *9* (67), 720–726.
- (47) Ibrahim, M.; Abuwatfa, W. H.; Awad, N. S.; Sabouni, R.; Husseini, G. A. Encapsulation, Release, and Cytotoxicity of Doxorubicin Loaded in Liposomes, Micelles, and Metal-Organic Frameworks: A Review. *Pharmaceutics* **2022**, *14* (2), 254.
- (48) Naumenko, V. A.; Vlasova, K. Yu.; Garanina, A. S.; Melnikov, P. A.; Potashnikova, D. M.; Vishnevskiy, D. A.; Vodopyanov, S. S.; Chekhonin, V. P.; Abakumov, M. A.; Majouga, A. G. Extravasating Neutrophils Open Vascular Barrier and Improve Liposomes Delivery to Tumors. *ACS Nano* **2019**, *13* (11), 12599–12612.
- (49) Zhang, H. Thin-Film Hydration Followed by Extrusion Method for Liposome Preparation. *Methods Mol. Biol.* **2017**, *1522*, 17–22.
- (50) Cherukuri, V.; Guo, T.; Schiff, S. J.; Monga, V. Deep MR Brain Image Super-Resolution Using Spatio-Structural Priors. *IEEE Trans. Image Process.* **2020**, *29*, 1368–1383.
- (51) Wu, H.; Yan, J. The Mechanism of Digitized Landscape Architecture Design under Edge Computing. *PLoS One* **2021**, *16* (9), No. e0252087.
- (52) Paxton, N. C.; Allenby, M. C.; Lewis, P. M.; Woodruff, M. A. Biomedical Applications of Polyethylene. *Eur. Polym. J.* **2019**, *118*, 412–428.
- (53) Zhao, H.; Zhang, L.; Zheng, S.; Chai, S.; Wei, J.; Zhong, L.; He, Y.; Xue, J. Bacteriostatic Activity and Cytotoxicity of Bacterial Cellulose-Chitosan Film Loaded with in-Situ Synthesized Silver Nanoparticles. *Carbohydr. Polym.* **2022**, *281*, No. 119017.
- (54) Shao, Z.; Chen, Y.; Jiang, J.; Xiao, Y.; Kang, G.; Wang, X.; Li, W.; Zheng, G. Multistage-Split Ultrafine Fluffy Nanofibrous Membrane for High-Efficiency Antibacterial Air Filtration. *ACS Appl. Mater. Interfaces* **2022**, *14* (16), 18989–19001.
- (55) Zhao, L.; Ren, Z.; Liu, X.; Ling, Q.; Li, Z.; Gu, H. A Multifunctional, Self-Healing, Self-Adhesive, and Conductive Sodium Alginate/Poly (Vinyl Alcohol) Composite Hydrogel as a Flexible Strain Sensor. *ACS Appl. Mater. Interfaces* **2021**, *13* (9), 11344–11355.
- (56) Zhang, W.; Khan, A.; Ezati, P.; Priyadarshi, R.; Sani, M. A.; Rathod, N. B.; Goksen, G.; Rhim, J. W. Advances in Sustainable Food Packaging Applications of Chitosan/Polyvinyl Alcohol Blend Films. *Food Chem.* **2024**, *443*, No. 138506.
- (57) Wu, S.; Shi, W.; Li, K.; Cai, J.; Xu, C.; Gao, L.; Lu, J.; Ding, F. Chitosan-Based Hollow Nanofiber Membranes with Polyvinylpyrrolidone and Polyvinyl Alcohol for Efficient Removal and Filtration of Organic Dyes and Heavy Metals. *Int. J. Biol. Macromol.* **2023**, *239*, No. 124264.